IEEE Photonics Journal
An IEEE Photonics Society Publication

Bloch Surface Wave Assisted Structured Illumination Microscopy for Sub-100 nm Resolution

Volume 13, Number 1, February 2021

Weijie Kong
Changtao Wang
Mingbo Pu
Xiaoliang Ma
Xiong Li
Xiangang Luo

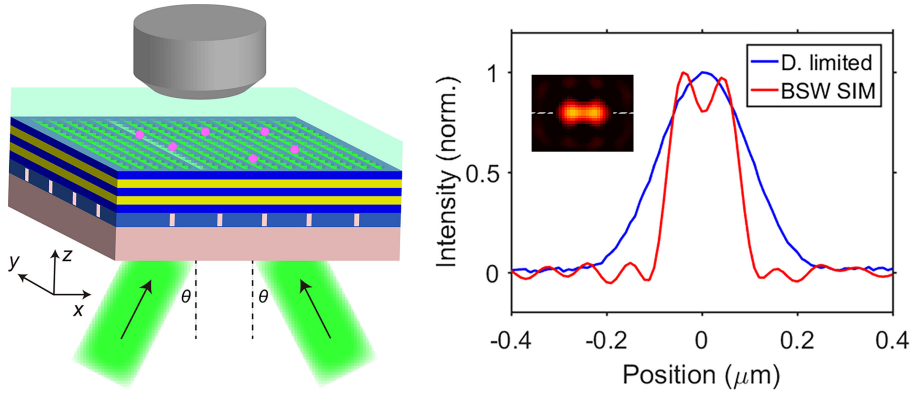

DOI: 10.1109/JPHOT.2020.3044920

Bloch Surface Wave Assisted Structured Illumination Microscopy for Sub-100 nm Resolution

Weijie Kong,[1,2] Changtao Wang,[1,2] Mingbo Pu,[1,2] Xiaoliang Ma,[1,2] Xiong Li,[1,2] and Xiangang Luo [1,2]

[1]State Key Laboratory of Optical Technologies on Nano-Fabrication and Micro-Engineering, Institute of Optics and Electronics, Chinese Academy of Sciences, Chengdu 610209, China
[2]School of Optoelectronics, University of Chinese Academy of Sciences, Beijing 100049, China

DOI:10.1109/JPHOT.2020.3044920

Manuscript received November 14, 2020; revised December 5, 2020; accepted December 11, 2020. Date of publication December 17, 2020; date of current version December 31, 2020. This work was supported in part by the National Natural Science Foundation of China under Grant 61805252, CAS "Light of West China" Program, Youth Innovation Promotion Association CAS, and in part by the Local Development Project of Science and Technology guided by the Central Government under Grant 2020ZYD021. Corresponding author: Xiangang Luo (e-mail: lxg@ioe.ac.cn).

Abstract: Structured illumination microscopy (SIM) is one of the most powerful and versatile super-resolution methods due to its live-cell imaging ability of subcellular structures with high speed. In this paper, we propose an alternative SIM assisted by Bloch surface wave (BSW). Through replacing the conventional laser interference fringes with sub-diffraction BSW counterparts with higher spatial frequency, the imaging resolution of SIM could be enhanced greatly and the super-resolution imaging capability down to 80 nm could be achieved. Compared with traditional wide-field fluorescence microscopy, this BSW SIM demonstrates 2.78 times enhancement in imaging resolution, which surpasses general SIM with only 2 times improvement. Moreover, the structured illumination intensity could be boosted drastically, which is beneficial to nonlinear super-resolution imaging techniques, such as saturated SIM. This BSW SIM would provide a super-resolution, wide field of view approach for surface super-resolution fluorescent imaging while maintaining high imaging speed and good bio-compatibility.

Index Terms: Fluorescence microscopy, Photonic crystals, Subwavelength structures.

1. Introduction

Bound by the optical diffraction limit, the conventional optical microscopy just achieves the limited spatial resolution of around 250 nm in lateral for visible light. This impedes the rapid progress of subcellular- and even molecular- biology, which requires sub-100 nm and even nano-scale optical imaging resolution, such as, observation of cell signaling pathways, immune responses, surface events during cell cycle and adhesion, movement of proteins, and calcium ions inside of live-cells. Moreover, the imaging speed must fulfill the requirement of living bio-specimen imaging. Overall, the microscopy which could simultaneously realize super-resolution, high speed, large field of view (FOV), and good bio-compatibility et al is in great demand.

The invention of stimulated emission depletion microscopy (STED) [1], [2] and single-molecule localization microscopy (SMLM) usher in an era of the super-resolution imaging technologies. By

employing the mechanisms that manage the fluorophores switching between on and off states, the classical optical resolution limit could be overcome, and the spatial resolution down to tens of nanometers could be realized as expected, which enables the possibility of exploring life secret in depth. Unfortunately, STED requires the ultra-high optical intensity for depleting fluorescent and the confocal scanning imaging style leads to the low imaging speed for specimens in a large area. As a result, the obvious phototoxicity and photobleaching, as well as low imaging speed restrict it to living cell applications. SMLM such as photoactivated localization microscopy (PALM) [3] and stochastic optical reconstruction microscopy (STORM) [4] obtains the super-resolution imaging capability by precise localization of individual fluorescent molecular, and requires capture several ten-thousands of original sub-images averagely for reconstructing one super-resolution image. Thus, the imaging speed is limited and SMLM is mainly adopted to fixed cells and specimens.

In parallel with these advancements, structured illumination microscopy (SIM) [5]–[7] has evolved into one of the most powerful and practical optical super-resolution imaging approaches, mainly because of it's high spatial/temporal resolution, low phototoxicity/photobleaching, as well as better bio-compatibility with live cells and specimens [8], [9]. In principle, under the illumination of structured light, such as Moiré fringe, the high spatial frequency information of the specimen could be shifted into the finite passband of the imaging system. After capturing a series of diffraction-limited sub-images, the super-resolution images could be reconstructed through reshifting the original high spatial frequency information to their initial positions. Notably, the imaging resolution of SIM is mainly determined by the spatial frequency of the illumination pattern and the numerical aperture (NA) of the objective lens. Traditionally, the structured illumination patterns with high spatial frequency are generated by the laser interference, and hence early SIM just achieves 2-times improvement of imaging resolution than standard optical microscopy. As a result, the spatial resolution of sub-100 nm could not be realized but is highly demanded all along. Although saturated SIM (SSIM) [10] could compress the resolution to tens of nanometers, the high illumination intensity demanded for fluorescence saturation would cause photobleaching and associated photoxicity, and the advantages of living cell imaging would lose.

In order to enhance the resolution of SIM, the spatial frequency of structured illumination pattern has been improved substantially by exploiting near field illumination module. Such as total internal reflection fluorescence (TIRF) based SIM (TIRF-SIM) [11], waveguide chip based SIM (cSIM) [12], plasmonic SIM (PSIM) [13], [14] and localized plasmonic SIM (LPSIM) [15]–[17]. For TIRF-SIM, the special objective lens with high NA must be required, meanwhile, the spatial frequency of the illumination interference fringe is limited by the refractive index n of objective lens and incident angle, so it is commonly smaller than $2nk_0$, where k_0 is wave vector in vacuum. cSIM is a two-dimensional SIM approach and reduces the footprint of the light illumination path of SIM, the spatial frequency could be enhanced to $3.38k_0$ [12], but the intensity of waveguide mode would decay along propagation direction, thus the imaging FOV is limited. PSIM could achieve higher spatial frequency by employing surface plasmon polariton (SPP), while the limited metal medium restricts the spatial frequency of illumination fringe, such as $2.88k_0$ for Air/Ag configuration [14]. On the contrary, LPSIM manifests an ability to attain higher spatial frequency of illumination pattern, however, speckle illumination patterns increase complexity and time consumption of the iterative reconstruction algorithm for super-resolution images [18].

In this paper, the SIM with deep subwavelength imaging resolution beyond 100 nm is proposed by employing Bloch surface wave (BSW) with sub-diffraction spatial frequency. BSW are surface electromagnetic modes excited at the interface between a truncated periodic dielectric multilayer with a photonic bandgap and its surrounding medium [19], [20], which is considered as the dielectric analogue of SPP [21]–[23]. Through carefully design one-dimensional photonic crystal (1D-PC), the evanescent Bloch wave lying photonic bandgap is launched. Under the symmetrical incident of two beams via two-dimensional square grating, the excited counter-propagating BSWs interfere with each other and the sub-diffraction interference fringes near the outgoing interface of 1D-PC are generated for structured illumination. Simulation results indicate that the spatial frequency could reach to $3.65k_0$ for the BSW interference fringes. After adopting the reconstruction algorithm for traditional SIM, the super-resolution images with resolution down to 80 nm could be achieved

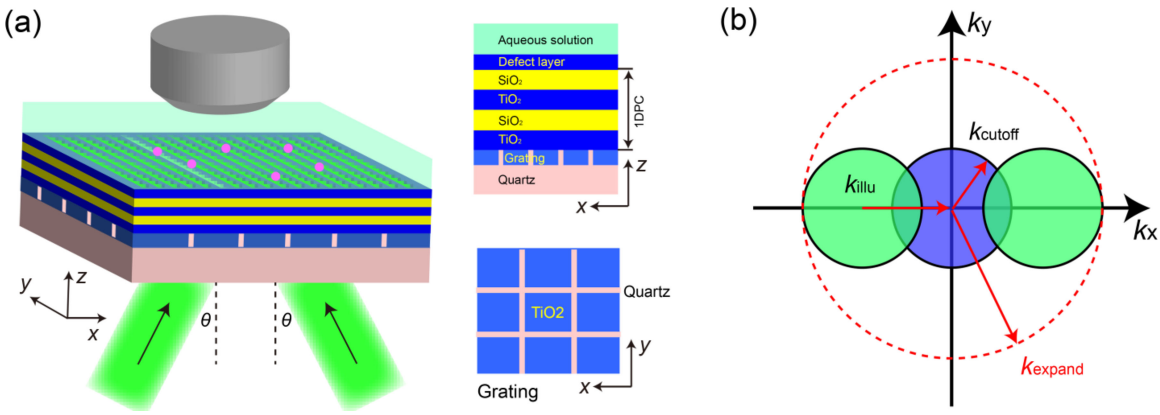

Fig. 1. BSW SIM imaging setup. (a) Schematic of grating loaded 1D-PC for exciting BSW. (b) Resolution improvement representation in spatial spectrum space. The blue circle represents the detectable low spatial frequency components, while the green circle represents the high spatial frequency components shifted by BSW SIM. The red dotted line corresponds to the total accessible spatial spectrum region of BSW SIM.

efficiently. Because of the evanescent characteristic of BSW, this approach could get ultra-thin optical sectioning capability in axial in the meanwhile. This BSW SIM method would pave a new way for super-resolution fluorescence imaging.

2. BSW Assisted SIM

As shown in Fig. 1(a), under the certain incident angle, the momentum between diffraction wave from grating and BSW is matched, thus the evanescent BSWs are excited and interfere with each other near the interface between the truncated outmost layer and surrounding medium (such as aqueous specimens). As a result, the sub-diffraction illumination fringes could be achieved, thus the fine information of object with higher spatial frequency could be moved into the detectable regime of optical imaging system, showing in Fig. 1(b). As a result, the better imaging resolution would be attained for SIM. Moreover, the phase of interference fringes could be adjusted by changing the phase difference between two incident beams. Through controlling polarization direction, the in-plane orientation of interference fringes could be easily altered. The flexible manipulation of fringes fulfils the requirements of SIM and the super-resolution images would be obtained combing with optical imaging system.

To support BSW with a subwavelength period, the 1D-PC is designed by optimizing, which is comprised of two pairs of alternative layers of TiO_2 and SiO_2, as well as an outmost TiO_2 layer. Except for the truncated TiO_2 layer, which is 60 nm, the thickness of other TiO_2 layers are 120 nm. Each SiO_2 layer has the same thickness of 157 nm. The surrounding medium on the BSW illumination side is an aqueous solution within bio-specimens. The refractive index of TiO_2, SiO_2, quartz and aqueous solution at the wavelength of 532 nm are $2.4958 + 0.0007i$, $1.4807 + 0.0004i$, 1.50, and 1.33, respectively.

The dispersion diagram of the semi-infinite underlying periodic TiO_2/SiO_2 multilayer under transverse electric (TE) polarized incidence is obtained by the transfer matrix method (TMM) [24] and is plotted in Fig. 2(a). The first blue band corresponds to the photonic bandgap of 1D-PC and a BSW would exist in this bandgap, which means BSW could not radiate in multilayer and surrounding aqueous solution. The dispersion relation of as-designed BSW is calculated [25] and displayed by a red dotted line. Meanwhile, light curves for aqueous solution and quartz substrate are also shown. Obviously, the BSW possesses a higher transverse wavevector than that of the light in aqueous solution. Further, the BSW dispersion relation strongly depends on the surrounding medium and the truncated topmost layer. Especially, the thickness of the truncated layer determines the location

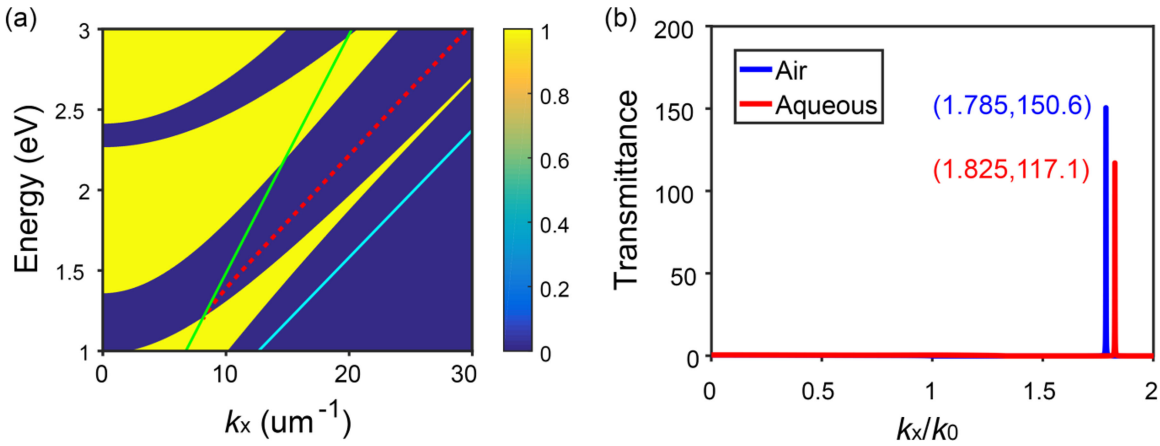

Fig. 2. BSW excitation. (a) Photonic bandgap and BSW dispersion relation (red dotted line) for semi-infinite periodic TiO_2/SiO_2 multilayer under the incidence of TE-polarized light. Light curves for the aqueous solution (green line) and quartz substrate (light blue line) are also shown. (b) Transmittance of TE-polarized light with different transverse wavevector (normalized by k_0).

of the dispersion curve of BSW. When increasing the thickness of the truncated layer, the BSW dispersion curve shifts towards the right edge of the photonic bandgap, meaning the higher spatial frequency of BSW. Under the half of thickness of the periodic TiO_2 layer, the BSW dispersion curve lies in the middle of the bandgap, and then the highest spatial frequency is attained, which is beneficial to super-resolution SIM. Raising the truncated layer thickness further, this 1D-PC would not sustain a BSW. At these conditions, for BSW at 532 nm (2.33 eV), the corresponding transverse wavevector reaches to 21.39 μm^{-1}, *i.e.*, $1.813k_0$. To get the transverse wavevector more accurately, the transmittance at 532 nm is calculated also by TMM and a sharp peak would appear, which is located in $k_x = 1.825k_0$ for aqueous solutions and $k_x = 1.785k_0$ for air, as shown in Fig. 2(b). It indicates the periods of BSW in aqueous solutions and air are respectively 292 nm and 298 nm. As we know, BSW could exist under both TE and TM (transverse magnetic) polarization. The reason for choosing TE polarization incidence in this text is as follows: (1) The spatial frequency under TE polarization is larger than that under TM polarization, (2) the interference fringe contrast under TE polarization is superior to that under TM polarization, which results from vanishing of electric field components along the orthogonal directions of interference fringe under TE polarization, which is another advantage compared with SPP under excitation of TM polarization.

In order to provide a large momentum for exciting BSW in 1D-PC, a two-dimensional square diffraction grating in a square lattice is selected. When employing the diffraction wave of 1st order from grating and setting the incident angle as $\pm 7.2°$, the grating period should be 325 nm for matching the momentum of BSW with $1.825k_0$. After carefully optimizing, the depth of 240 nm and the duty cycle of 0.7 are obtained for TiO_2 grating. It is noteworthy that the two-dimensional design of grating is to adjust the polarization direction of the incident beam and then the in-plane illumination orientation of fringes conveniently.

3. Results and Discussion

The field distributions of BSW could be obtained from COMSOL Multiphysics simulations [26]. Under single TE-polarized light incidence with the matched angle of 7.2°, the electric field E_y map normalized by incident electric field E_0 in *xz* cross-section could be attained, which is shown in Fig. 3(a). It is clear that the sub-diffraction surface wave is launched in 1D-PC. Moreover, the normalized electric field and the corresponding intensity is enhanced and confined drastically in the outmost truncated layer near the surrounding, as illustrated in Fig. 3(b). Further, Fig. 3(c) shows that optical intensity decays exponentially in the aqueous solution and oscillates damply in the

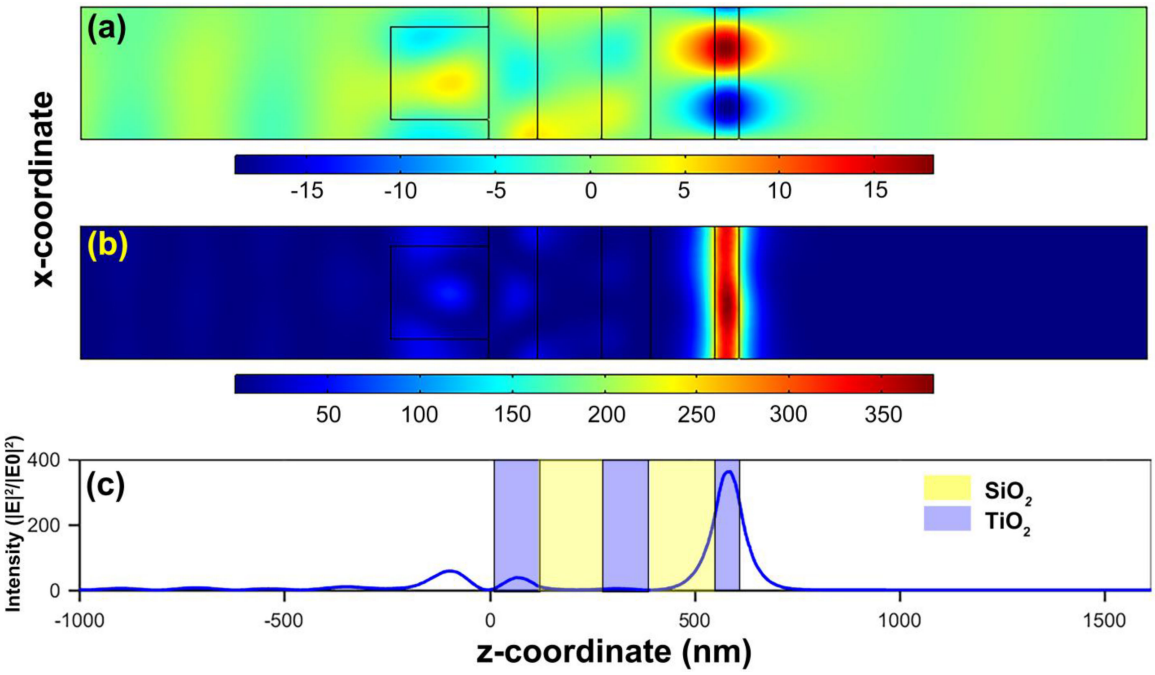

Fig. 3. Electric field maps and the corresponding intensity profiles for BSW excited by 2D square grating. Maps of (a) E_y and (b) Intensity ($|E|^2/|E_0|^2$) in *xz* cross-section of the multilayer. (c) Line intensity ($|E|^2/|E_0|^2$) profile along *z*-direction.

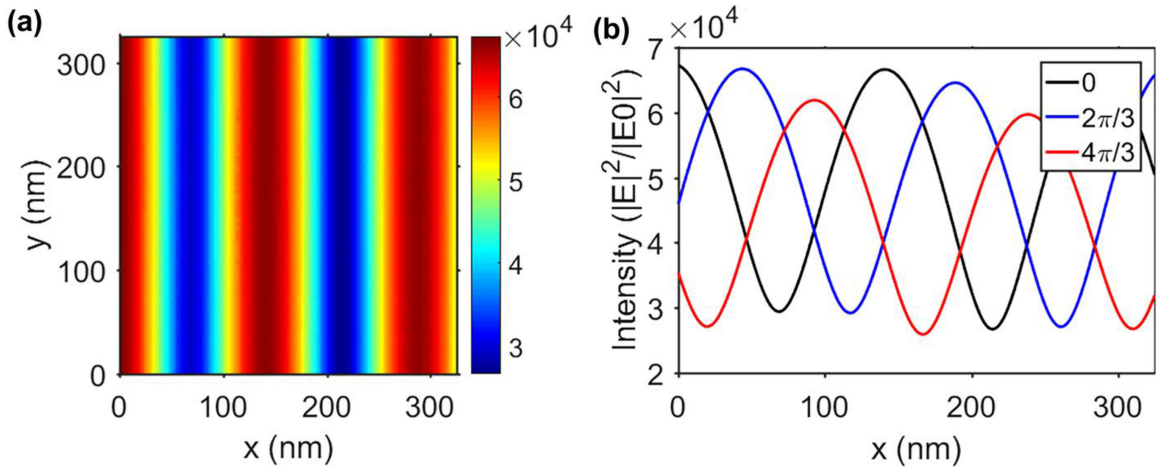

Fig. 4. interference intensity profiles for BSW excited by 2D square grating. (a) Interference fringe in illumination plane (*xz*) away 20 nm from the topmost layer of the multilayer. (b) Interference intensity ($|E|^2/|E_0|^2$) profiles with the phase difference of 0, $2\pi/3$ and $4\pi/3$.

1D-PC, which is an obvious signature of the presence of BSW. The intensity enhancement factor could reach 364, which is very beneficial to nonlinear SIM [10] requiring an ultra-high illumination light.

When two TE-polarized light beams impinge on the 2D exciting grating with $\pm 7.2°$, two counter-propagating BSWs are generated and interfere with each other along the truncated layer, and thus a 1D subwavelength standing wave for SIM are produced. Fig. 4(a) displays the normalized intensity

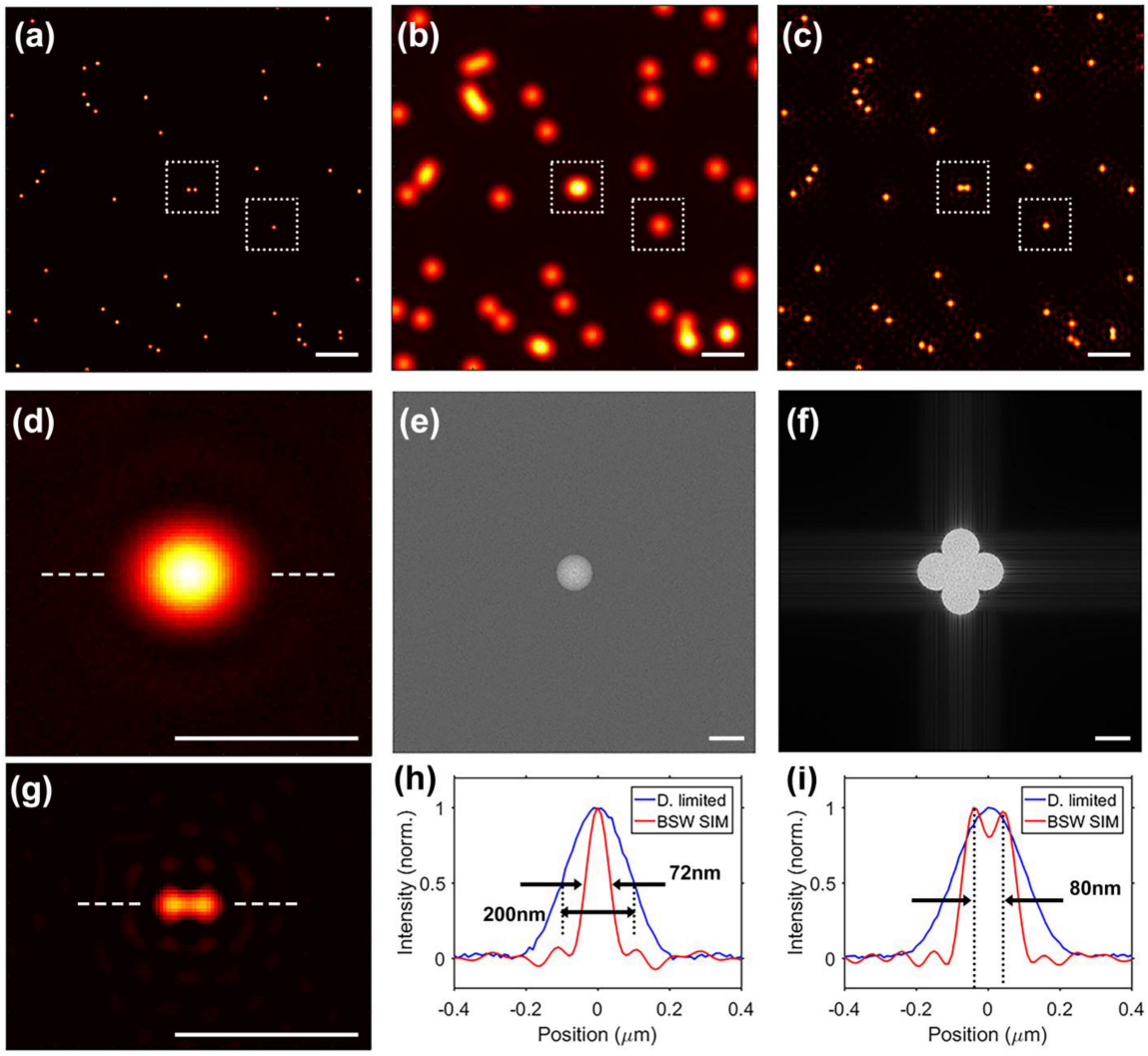

Fig. 5. Demonstration of BSW SIM imaging capability. (a) Ground truth image of a distribution of fluorescent microspheres with 40 nm diameter. (b) Conventional diffraction-limited image of (a). (c) BSW SIM image. (e) and (f) are the magnitude of Fourier transforms of images in (b) and (c), respectively. (d) and (g) are the diffraction-limited image and the SIM image of the selected central boxes in (b) and (c), respectively. Normalized intensity profile of image of (h) a single microsphere and (i) two closed microspheres with 80 nm center distance in the selected boxes. Scale bar is 500 nm for (a), (b), (c), (d) and (g). Scale bar is 5 μm^{-1} for (e) and (f).

distribution in the illumination plane away 20 nm from the topmost layer of 1D-PC, demonstrating the uniform interference fringe is indeed produced as expected. When the polarization direction of two incident beams is rotated as 90°, the intensity distribution in the illumination plane is nearly the same as the distribution showing in Fig. 4(a) but the fringe orientation would be rotated as 90° as well. The corresponding intensity profiles across interference fringe with different phase differences are shown in Fig. 4(b). One can acquire that the period of this interference fringe is about 146 nm, which is 1/3.64 times of incident wavelength. Besides, the fringe contrast exceeds 0.4, meeting the requirements for SIM [27]. By employing these sub-diffraction fringes for structured illumination, three diffraction-limited sub-images could be captured for each in-plane illumination orientation.

Finally, the super-resolution imaging performance of BSW SIM is verified through simulations. Dispersive fluorescent microspheres with 40 nm diameter serve as ground truth object (Fig. 5(a))

for imaging, the minimum center-to-center distance is set as 80 nm for testifying the imaging resolution. Meanwhile, its excitation and emission wavelengths are $\lambda_{\rm ex} = 532$ nm and $\lambda_{\rm em} = 560$ nm, respectively. After conventional imaging with $NA = 1.45$ objective lens and 5% Gaussian noise added, the diffraction-limited image is obtained, as shown in Fig. 5(b). Two closed fluorescent microspheres merge into one spot, the reason is that the achieved imaging resolution could not reach to 80 nm. On the contrary, through adopting the BSW structured illumination with also 5% Gaussian noise added and the corresponding SIM reconstruction algorithm [28], [29], the imaging resolution could be enhanced drastically, as revealed by Fig. 5(c). Especially, from the magnified images of two closed fluorescent microspheres (Fig. 5(g)) in the central selected box in Fig. 5(c), one can distinguish two microspheres clearly after BSW SIM while can not in the conventional imaging. The Fourier domain of the conventional image (Fig. 5(e)) and SIM image (Fig. 5(f)) could explain this. It is evident that the cutoff spatial frequency of the imaging system is extended to 2.32 times. For a more quantitative illustration, Fig. 5(h) shows the transverse cut of the super-resolution image of a single microsphere (Fig. 5(d)), and also compares it with that of the corresponding diffraction-limited image. The full width at half maxima (FWHM) of single microsphere image is compressed from 200 nm to 72 nm, yielding a 2.78-fold resolution improvement. The counterpart for two-closed microspheres is illustrated in Fig. 5(i). It is more obvious that two closed microspheres with a center-to-center distance of 80 nm could be clearly resolved via BSW SIM. This confirms that the sub-diffraction imaging resolution of 80 nm could be achieved, which is in good agreement with the theoretical prediction of 83 nm, calculated by $\lambda_{\rm em}/(2NA + 2\lambda_{\rm em}/\lambda_{\rm BSW})$. Under current design, the orientations of illumination fringe are just 0° and 90°, thus the gaps would appear in Fourier space with relevant information missing near 45° orientation, which needs to be solved in the following work.

In comparison with conventional SIM, BSW SIM could suppress out-of-focus fluorescence effectively and then provide a high signal-to-noise ratio (SNR) because of the evanescent nature of BSW. For BSW with a transverse wavevector of $1.825k_0$ in aqueous solutions, the evanescent field penetration depth is about 68 nm, which is smaller than that of TIRF microscopy. This means the optical sectioning [30] capability near the BSW illumination surface could be achieved. This good property makes BSW SIM suitable for studying the dynamic molecular behaviors of proteins bounded by plasma membrane and the labelled biomolecules on plasma membrane in vivo, such as vesicle endocytosis and exocytosis [31], [32], plasma membrane heterogeneity [33], protein stoichiometry [34], neuron structure [35] and cell growth [36]. The investigations of cell plasma membrane are much valuable for understanding the structures and functions of bio-specimens because many basic cellular processes occur in the cell plasma membrane with complex mechanisms.

Among the evanescent wave/mode illuminated SIM methods, BSW SIM has its own advantages. First, BSW could reach to higher transverse wavevector than that of surface plasmon wave and thus the imaging resolution could be enhanced. Second, the imaging FOV could be easily expanded by only enlarging the size of excitation grating and illumination beam. Third, the illumination intensity could be improved drastically, which would be a good choice for SSIM and other nonlinear based super-resolution imaging approaches. Certainly, BSW SIM has some limitations. The excitation conditions for BSW are rigorous, which requires the excitation light path should be carefully adjusted. Further, fabrication error for grating-loaded 1D-PC should be limited in a certain range. The detailed comparison among the typical near-field SIM methods is illustrated in Table 1.

BSW could be also employing for label-free surface-sensitive high-resolution imaging, which is named as BSW Microscopy (BSWM) [38]. When BSWs are used as the optical source to illuminate the specimens placed on the 1D-PC, the scattering signals from the specimens could be collected for label-free and real-time imaging. But its imaging resolution is only several hundreds nanometers, which means the super-resolution imaging capability could not be achieved. As for our BSW assisted SIM, the specimen for imaging needs to be fluorescent-labelled while the subdiffraction imaging resolution of sub-100 nm could be attained.

TABLE 1
Comparison Among the Typical Near-Field SIM Methods

	cSIM [12]	PSIM [14]	LPSIM [16]	BSW SIM
Resolution enhancement factor	~2.3	~2.6	~3.0	~2.78
Illumination wave vector	~3.38k_0	~2.88k_0	2.70~6.75k_0	~3.65k_0
Numerical aperture (NA)	1.2	1.0	1.2	1.45
Emission wavelength	690 nm	593 nm	500 nm	560 nm
SIM reconstruction algorithm	Fair-SIM [37]	Blind-SIM [18]	Blind-SIM [18]	Open-SIM [28]
Temporal resolution	high	low	low	high

4. Conclusion

In summary, we have presented another super-resolution imaging approach – Bloch Surface Wave based Structured Illumination Microscopy (BSW SIM). Through adopting 1D-PC, the BSW in photonic bandgap with high transverse wavevector could be launched. After interfering with counter-propagating BSWs, the subwavelength fringes could be generated for structured illumination. Combined with the conventional reconstruction algorithm, the super-resolution images could be attained. Simulation results show that BSW SIM manifests an ability to achieve higher imaging resolution than conventional SIM, and shows a 2.78 times enhancement in imaging resolution. This BSW SIM may find valuable applications in the field of real-time super-resolution biomedical imaging.

References

[1] T. A. Klar, S. Jakobs, M. Dyba, A. Egner, and S. W. Hell, "Fluorescence microscopy with diffraction resolution barrier broken by stimulated emission," *Proc. Nat. Acad. Sci.*, vol. 97, no. 15, pp. 8206–8210, 2000.
[2] K. I. Willig, B. Harke, R. Medda, and S. W. Hell, "STED microscopy with continuous wave beams," *Nat. Methods*, vol. 4, no. 11, pp. 915–918, 2007.
[3] S. T. Hess, T. P. K. Girirajan, and M. D. Mason, "Ultra-high resolution imaging by fluorescence photoactivation localization microscopy," *Biophysical J.*, vol. 91, no. 11, pp. 4258–4272, 2006.
[4] M. J. Rust, M. Bates, and X. Zhuang, "Sub-diffraction-limit imaging by stochastic optical reconstruction microscopy (STORM)," *Nat. Methods*, vol. 3, no. 10, pp. 793–796, 2006.
[5] M. G. L. Gustafsson, "Surpassing the lateral resolution limit by a factor of two using structured illumination microscopy," *J. Microsc.*, vol. 198, no. 2, pp. 82–87, 2000.
[6] J. R. Allen, S. T. Ross, and M. W. Davidson, "Structured illumination microscopy for superresolution," *Chemphyschem*, vol. 15, no. 4, pp. 566–576, 2014.
[7] F. Ströhl and C. F. Kaminski, "Frontiers in structured illumination microscopy," *Optica*, vol. 3, no. 6, pp. 667–677, 2016.
[8] P. Kner, B. B. Chhun, E. R. Griffis, and L. Winoto, and M. G. L. Gustafsson, "Super-resolution video microscopy of live cells by structured illumination," *Nat. Methods*, vol. 6, no. 5, pp. 339–342, 2009.
[9] Y. Hirano, A. Matsuda, and Y. Hiraoka, "Recent advancements in structured-illumination microscopy toward live-cell imaging," *Microscopy*, vol. 64, no. 4, pp. 237–249, 2015.
[10] M. G. L. Gustafsson, "Nonlinear structured-illumination microscopy: Wide-field fluorescence imaging with theoretically unlimited resolution," *Proc. Nat. Acad. Sci. United States America*, vol. 102, no. 37, pp. 13081–13086, 2005.
[11] D. Li *et al.*, "Extended-resolution structured illumination imaging of endocytic and cytoskeletal dynamics," *Science*, vol. 349, no. 6251, 2015, Art. no. aab3500.
[12] Ø. I. Helle, F. T. Dullo, M. Lahrberg, J.-C. Tinguely, O. G. Hellesø, and B. S. Ahluwalia, "Structured illumination microscopy using a photonic chip," *Nat. Photon.*, vol. 14, no. 7, pp. 431–438, 2020.
[13] F. Wei and Z. Liu, "Plasmonic structured illumination microscopy," *Nano Lett.*, vol. 10, no. 7, pp. 2531–2536, 2010.
[14] F. Wei *et al.*, "Wide field super-resolution surface imaging through plasmonic structured illumination microscopy," *Nano Lett.*, vol. 14, no. 8, pp. 4634–4639, 2014.
[15] J. L. Ponsetto, F. Wei, and Z. Liu, "Localized plasmon assisted structured illumination microscopy for wide-field high-speed dispersion-independent super resolution imaging," *Nanoscale*, vol. 6, no. 11, pp. 5807–5812, 2014.

[16] J. Ponsetto *et al.*, "Experimental demonstration of localized plasmonic structured illumination microscopy," *ACS Nano*, vol. 11, no. 6, pp. 5344–5350, 2017.
[17] A. Bezryadina, J. Zhao, Y. Xia, X. Zhang, and Z. Liu, "High spatiotemporal resolution imaging with localized plasmonic structured illumination microscopy," *ACS Nano*, vol. 12, no. 8, pp. 8248–8254, 2018.
[18] E. Mudry *et al.*, "Structured illumination microscopy using unknown speckle patterns," *Nat. Photon.*, vol. 6, no. 5, pp. 312–315, 2012.
[19] R. D. Meade, K. D. Brommer, A. M. Rappe, and J. D. Joannopoulos, "Electromagnetic bloch waves at the surface of a photonic crystal," *Phys. Rev. B*, vol. 44, no. 19, pp. 10961–10964, 1991.
[20] P. Yeh, "Electromagnetic propagation in periodic stratified media. I. General theory," *J. Opt. Soc. Amer.*, vol. 67, no. 4, pp. 423–438, 1977.
[21] M. I. Stockman *et al.*, "Roadmap on plasmonics," *J. Opt.*, vol. 20, no. 4, 2018, Art. no. 043001.
[22] Q. Sun, H. Yu, K. Ueno, S. Zu, Y. Matsuo, and H. Misawa, "Revealing the plasmon coupling in gold nanochains directly from the near field," *Opto-Electron. Adv.*, vol. 2, no. 4, 2019, Art. no. 180030.
[23] X. Luo, "Engineering optics 2.0: A revolution in optical materials, devices, and systems," *ACS Photon.*, vol. 5, no. 12, pp. 4724–4738, 2018.
[24] Z. Li and L. Lin, "Photonic band structures solved by a plane-wave-based transfer-matrix method," *Phys. Rev. E*, vol. 67, no. 4, 2003, Art. no. 046607.
[25] M. Liscidini and J. E. Sipe, "Analysis of Bloch-surface-wave assisted diffraction-based biosensors," *J. Opt. Soc. America B-Opt. Phys.*, vol. 26, no. 2, pp. 279–289, 2009.
[26] V. Koju, "Computational modeling of bloch surface waves in one-dimensional periodic and aperiodic multilayer structures," Ph.D. dissertation, Fac. Comput. Sci. Program, Middle Tennessee State Univ., Murfreesboro, 2017.
[27] J. Demmerle *et al.*, "Strategic and practical guidelines for successful structured illumination microscopy," *Nat. Protoc.*, vol. 12, no. 5, pp. 988–1010, 2017.
[28] A. Lal, C. Shan, and P. Xi, "Structured illumination microscopy image reconstruction algorithm," *IEEE J. Sel. Topics Quantum Electron.*, vol. 22, no. 4, pp. 50–63, Jul./Aug. 2016.
[29] [Online]. Available: https://github.com/LanMai/OpenSIM/tree/master/TIRFbasic
[30] W. Liu *et al.*, "Breaking the axial diffraction limit: A guide to axial super-resolution fluorescence microscopy," *Laser Photon. Rev.*, vol. 12, no. 8, 2018, Art. no. 1700333.
[31] M. W. Allersma, L. Wang, D. Axelrod, and R. W. Holz, "Visualization of regulated exocytosis with a granule-membrane probe using total internal reflection microscopy," *Mol. Biol. Cell*, vol. 15, no. 10, pp. 4658–4668, 2004.
[32] J. G. Burchfield, J. A. Lopez, K. Mele, P. Vallotton, and W. E. Hughes, "Exocytotic vesicle behaviour assessed by total internal reflection fluorescence microscopy," *Traffic*, vol. 11, no. 4, pp. 429–439, 2010.
[33] S. Yang, A. J. B. Kreutzberger, V. Kiessling, B. K. Ganserpornillos, J. M. White, and L. K. Tamm, "HIV virions sense plasma membrane heterogeneity for cell entry," *Sci. Adv.*, vol. 3, no. 6, 2017, Art. no. e1700338.
[34] M. C. Leake, J. H. Chandler, G. H. Wadhams, F. Bai, R. M. Berry, and J. P. Armitage, "Stoichiometry and turnover in single, functioning membrane protein complexes," *Nature*, vol. 443, no. 7109, pp. 355–358, 2006.
[35] I. Azoulayalfaguter *et al.*, "The tyrosine phosphatase SHP-1 promotes t cell adhesion by activating the adaptor protein CrkII in the immunological synapse," *Sci. Signaling*, vol. 10, no. 491, 2017, Art. no. eaal2880.
[36] C. Billaudeau *et al.*, "Contrasting mechanisms of growth in two model rod-shaped bacteria," *Nat. Commun.*, vol. 8, no. 1, 2017, Art. no. 15370.
[37] M. Müller, V. Mönkemöller, S. Hennig, W. Hübner, and T. Huser, "Open-source image reconstruction of super-resolution structured illumination microscopy data in imageJ," *Nat. Commun.*, vol. 7, no. 1, pp. 10980, 2016.
[38] Y. Kuai *et al.*, "Label-free surface-sensitive photonic microscopy with high spatial resolution using azimuthal rotation illumination," *Sci. Adv.*, vol. 5, no. 3, 2019, Art. no. eaav5335.